ELSEVIER

Materials Science and Engineering A 380 (2004) 272–280

MATERIALS SCIENCE & ENGINEERING A

www.elsevier.com/locate/msea

The out-of-plane compressive behavior of metallic honeycombs

F. Côté [a], V.S. Deshpande [a], N.A. Fleck [a,*], A.G. Evans [b]

[a] *Cambridge University Engineering Department, Trumpington Street, Cambridge, CB2 1PZ, UK*
[b] *Materials Department, University of California, Santa Barbara, CA 93106-5050, USA*

Received 24 September 2003; received in revised form 23 March 2004

Abstract

Stainless steel square-honeycombs have been manufactured by slotting together steel sheets and then brazing the assembly. Their out-of-plane compressive response has been measured as a function of the relative density, the ratio of specimen height to cell size, and the degree of constraint associated with bonding of the honeycomb to face-sheets. It has been found that, for the practical range of relative densities (less than 20%), the peak strength is relatively insensitive to both the ratio of the specimen height to cell size and to the presence or absence of bonding to face-sheets. An analytical model, derived from existing models for the buckling of shells, for elastic and plastic buckling of the square-honeycombs is shown to be in good agreement with the experimental measurements.

Keywords: Honeycombs; Plastic buckling; Energy absorption; Sandwich panels

1. Introduction

Hexagonal-honeycombs are routinely employed as cores for lightweight sandwich panels, as well as for energy absorption. They are typically manufactured from aluminum (Al) alloys by an in-plane expansion process that results in two of the six cell walls having double thickness [1]. This manufacturing method is restricted to relative density, $\bar{\rho} \leq 0.03$. In out-of-plane crushing, these honeycombs exhibit a stress peak followed by large stress oscillations associated with a succession of plastic folds in each cell. The peak is set by elastic buckling while the post-peak average strength, σ_m, is governed by folding of the cell walls and for a honeycomb made from an ideally plastic material is given by [1].

$$\Sigma \equiv \frac{\sigma_m}{\sigma_y \bar{\rho}} \approx 3.2\bar{\rho}^{2/3}, \tag{1a}$$

where σ_y is the yield strength of the parent material.

Recent studies [3,4] suggest that square-honeycomb cores having higher relative density would be preferable for high severity loadings, such as shocks, because of their combination of crushing resistance and in-plane stretching strength. The out-of-plane mean crushing strength of square-honeycombs made from an ideally plastic material is estimated to be

$$\Sigma \equiv \frac{\sigma_m}{\sigma_y \bar{\rho}} \approx 1.5\bar{\rho}^{2/3}, \tag{1b}$$

from the folding analysis [2] of an isolated square tube. Enhancements in the performance of square-honeycombs are expected upon using materials with high strain hardening, such as stainless steels. Motivated by these expectations, the present study examines the out-of-plane crushing characteristics of stainless steel square-honeycombs, exploring the sensitivity of the strength to such variables as: (i) the relative density, (ii) cell aspect ratio, (iii) degree of end constraint on the cells, and (iv) strain hardening of the cell wall material. Tests are performed using 304 stainless steel.

The outline of the paper is as follows. First, the procedure used to manufacture stainless steel square-honeycombs is described. Second, their out-of-plane compressive behavior is experimentally investigated, including the effects of relative density, cell aspect ratio, and bonding to face-sheets. It is shown that the peak strength is dictated by elastic or plastic buckling of the cell walls. Buckling models are presented and the predictions are compared with the measurements. Finally, the crushing response is compared with that for commercially available aluminum hexagonal-honeycombs, and with several alternative core topologies.

* Corresponding author. Tel.: +44-1223-332650; fax: +44-1223-332662.
E-mail address: naf1@eng.cam.ac.uk (N.A. Fleck).

0921-5093/$ – see front matter © 2004 Elsevier B.V. All rights reserved.
doi:10.1016/j.msea.2004.03.051

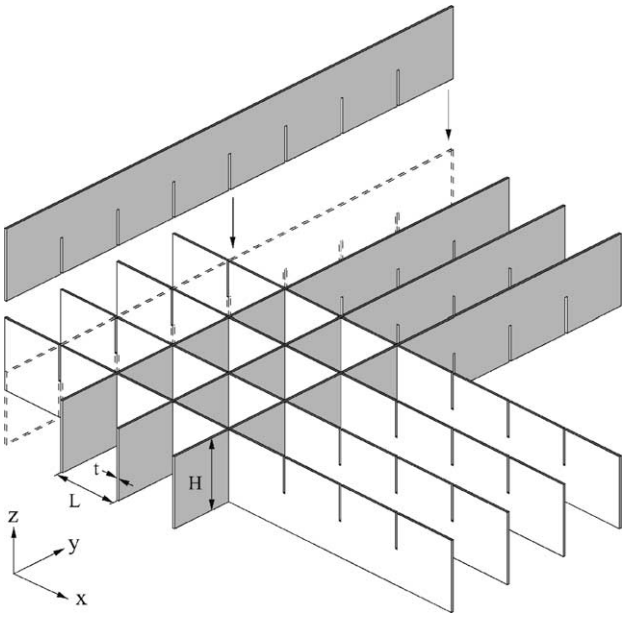

Fig. 1. Sketch of the square-honeycomb manufacturing technique.

2. Materials and manufacturing route

Square-honeycombs were manufactured from 304 stainless steel sheets, thickness $t = 0.490$ mm. The sheets were cropped into rectangles, height H in the range 2.8–163.5 mm and length of 17.6–196.2 mm. Cross-slots (Fig. 1), width $\Delta t = 0.495$ mm, and spacing L in the range 2.8–32.7 mm, were cut by electro-discharge machining (EDM) and the square-honeycomb was assembled as sketched in Fig. 1. The clearance of 5 μm between sheet and slot facilitated assembly while providing a sufficiently tight fit to assure stability. Brazing was conducted with Ni–Cr 25-P10 (wt.%) at 1120 °C in dry argon at 0.03–0.1 mbar and the braze was applied uniformly over the sheets, which increased the sheet thickness to $t = 0.5$ mm. Capillarity draws the braze into the joints, resulting in an excellent bond. In some cases, 304 stainless steel face-sheets, thickness 3 mm, were bonded to the top and bottom of the square-honeycomb. The relative density $\bar{\rho}$ of the square-honeycomb is to first order given by

$$\bar{\rho} = \frac{2t}{l}. \tag{2}$$

Table 1
Geometry of the square-honeycombs manufactured and tested in this study.

Wall thickness (t, mm)	Cell size, (L, mm)	Relative density ($\bar{\rho}$)
0.50	32.7	0.03
0.50	19.6	0.05
0.50	9.8	0.10
0.50	4.9	0.20
0.50	2.8	0.36

An example of a manufactured square-honeycomb, with $\bar{\rho} = 0.03$, comprising 6×6 cells and a cell aspect ratio $H/L = 5$ is shown in Fig. 2. The cell sizes and relative densities of the square-honeycombs manufactured in this study are listed in Table 1. Five relative densities were manufactured in four configurations:

(1) Aspect ratio $H/L = 5$, with the top and bottom faces of the square-honeycomb bonded to 3-mm-thick 304 stainless steel face-sheets;
(2) Aspect ratio $H/L = 5$, unbonded;

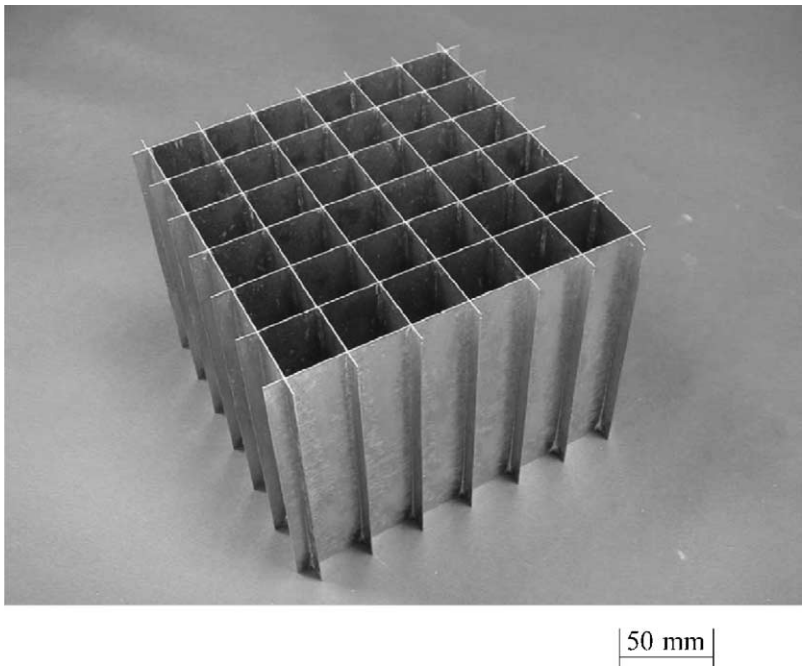

Fig. 2. Photograph of the unbonded $\bar{\rho} = 0.03$ stainless steel square-honeycomb with a cell aspect ratio $H/L = 5$.

(3) Aspect ratio $H/L = 1$, with the top and bottom faces of the square-honeycomb bonded to 3-mm-thick 304 stainless steel face-sheets;
(4) Aspect ratio $H/L = 1$, unbonded.

Thus, a wide range of relative densities and specimen configurations are investigated to determine the deformation mechanism of square-honeycombs. Most specimens comprised 6×6 cells. A few tests were performed with specimens comprising 12×12 cells to examine edge effects. All properties were measured at a strain rate $10^{-4}\,s^{-1}$, using a laser extensometer to measure the average compressive strain in the out-of-plane direction (z-direction in Fig. 1).

3. Mechanical measurements

3.1. The parent material

Tensile specimens of dog-bone geometry were cut from the as-received 304 stainless steel sheets and subjected to the same brazing cycle used to manufacture the square-honeycombs. The measured true tensile stress versus logarithmic strain response, shown in Fig. 3, may be approximated as an elastic, linearly hardening solid: Young's modulus $E = 210\,GPa$, yield strength $\sigma_y = 210\,MPa$, and linear hardening modulus $E_t = 2.1\,GPa$.

3.2. Compression of steel square-honeycombs

The measured out-of-plane compressive responses of the square-honeycombs are shown in Figs. 4–6 for the relative densities $\bar{\rho}$ of 0.03, 0.10, and 0.20, respectively. The $\bar{\rho} = 0.03$ and 0.10 specimens display a peak strength followed by softening and, finally rapid hardening upon densification at a strain, $\varepsilon_D \approx 0.6$–$0.7$. The softening beyond the peak is more abrupt when $H/L = 5$ and the responses are largely unaffected by either bonding to the face sheets (Figs. 4 and 5) or by the number of cells (Fig. 5). The two exceptions are: (i) the diminished densification strain found in the bonded specimens at $H/L = 1$, attributed to the excess braze material at the nodes, and (ii) a slightly lower load-carrying capacity for specimens with 6×6 cells, when $H/L = 5$, caused by tearing of the brazed joints near the periphery of the specimen. Conversely, when $\bar{\rho} = 0.20$ (Fig. 6), the response is strongly affected by bonding to face-sheets. For $H/L = 1$ (Fig. 6a), bonding eliminates the stress peak, while for $H/L = 5$ (Fig. 6b), it elevates the peak by about 20%.

The variation of the peak strength σ_p with relative density $\bar{\rho}$, plotted in Fig. 7, is compared with the mean stress prediction from Eq. (1b), at the equivalent yield strength, $\sigma_y = 210\,MPa$. Note that, while the power-law dependence

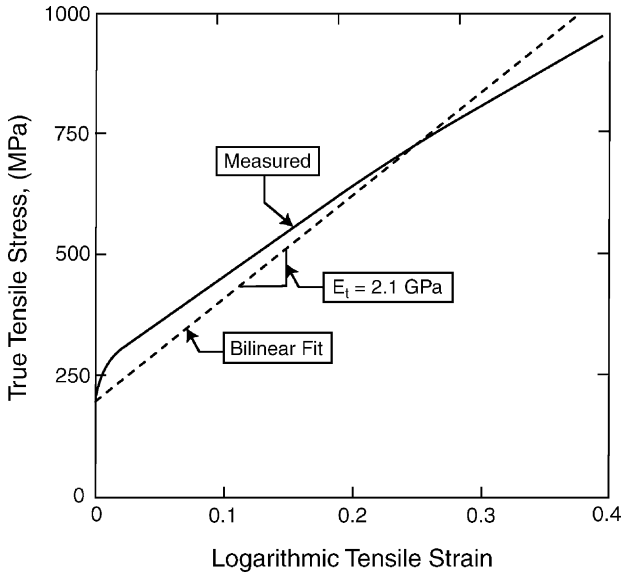

Fig. 3. Measured tensile stress vs. strain curve of the as-brazed 304 stainless steel. A bilinear fit with the choices $\varepsilon_y = 0.1\%$, $\sigma_y = 210\,MPa$ and a linear hardening modulus $E_t = 2.1\,GPa$ is also shown as a dashed line.

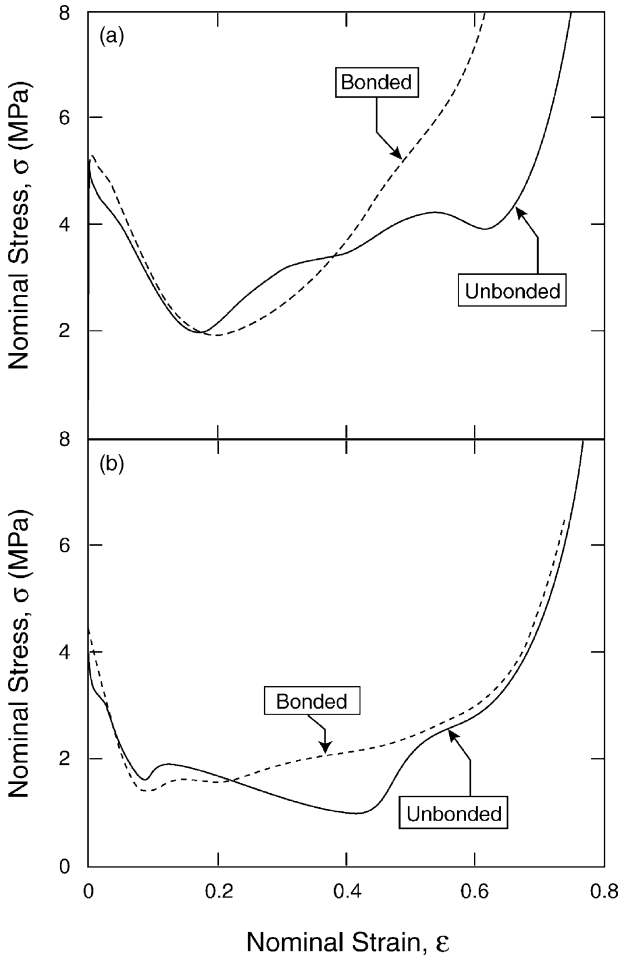

Fig. 4. Out-of-plane compressive stress vs. strain response of the $\bar{\rho} = 0.03$ square-honeycombs with cell aspect ratios (a) $H/L = 1$ and (b) $H/L = 5$. In each case, curves are shown for honeycombs that are bonded and not bonded to face-sheets.

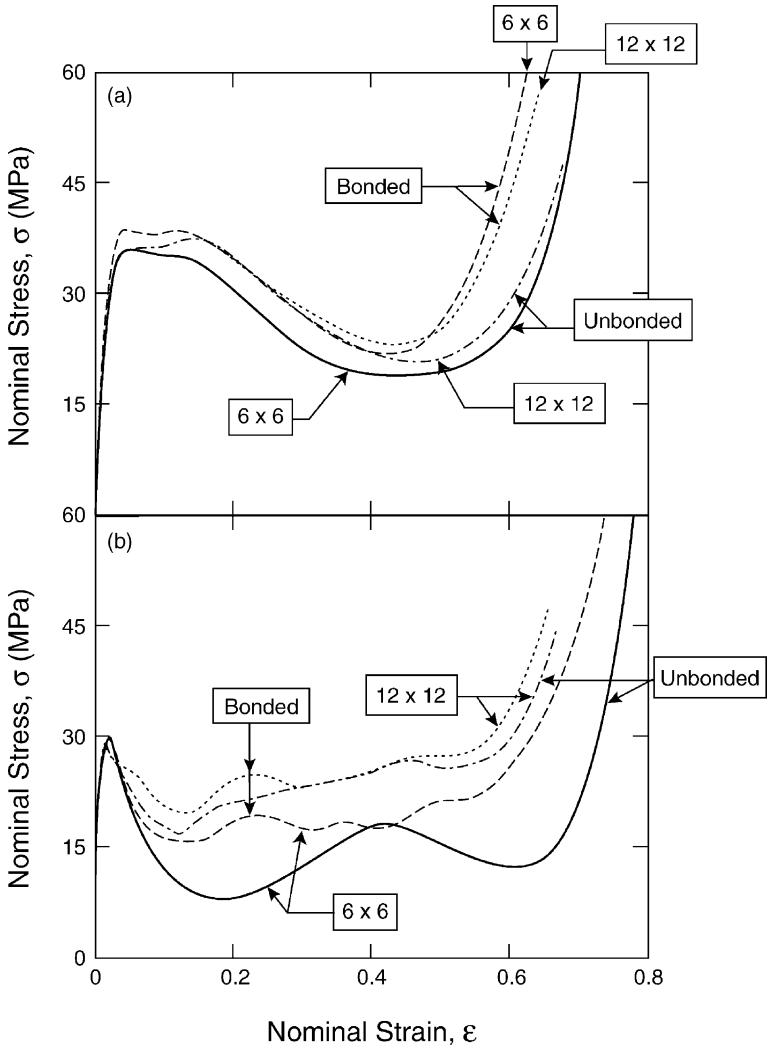

Fig. 5. Out-of-plane compressive stress vs. strain response of the $\bar{\rho} = 0.10$ square-honeycombs with cell aspect ratios (a) $H/L = 1$ and (b) $H/L = 5$. In each case, curves are shown for 6×6 and 12×12 cell honeycombs that are bonded to and not bonded to face-sheets.

of peak strength upon $\bar{\rho}$ is consistent with Eq. (1b), the coefficient is larger by a factor of about four.

An image of the unbonded $\bar{\rho} = 0.10$, 12×12 cells specimen ($H/L = 5$), compressed to a strain of $\varepsilon \approx 0.10$ (Fig. 8) reveals periodic, axial-torsional buckling of the cells. In this mode, the vertical nodal axis remains straight, while cell wall segments rotate about this axis. We demonstrate that this specimen underwent plastic buckling by comparing the true stress σ_w versus logarithmic strain ε_w developed in a cell wall with the uniaxial response of the parent material. For this purpose, the wall stress σ_w and strain ε_w are estimated using

$$\sigma_w = \frac{\sigma_n}{\bar{\rho}}(1 - \varepsilon_n) \tag{3a}$$

and

$$\varepsilon_w = |\ln(1 - \varepsilon_n)|, \tag{3b}$$

respectively. Here, σ_n is the nominal compressive stress in the honeycomb at a compressive nominal strain ε_n (all stress and strain measures are taken to be positive). The comparison (Fig. 9) demonstrates that the cell wall response duplicates that for the parent material up to the peak stress, coincident with the onset of plastic buckling, and deviates thereafter.

3.3. Compression of Al alloy hexagonal-honeycombs

Measurements of the out-of-plane compressive response of a commercial Al alloy hexagonal-honeycomb, HexWeb[1], are obtained (without bonding the honeycomb to face-sheets), and contrasted with the steel square-honeycomb. The HexWeb material is made from a 3003-grade aluminum alloy (yield strength, $\sigma_y \approx 210$ MPa), manufactured by cold expansion, at three relative densities $\bar{\rho} = 0.018$, 0.024, and 0.03. The response of the $\bar{\rho} = 0.03$ hexagonal-honeycomb is compared with that

[1] Hexcel Composites, Duxford, Cambridge, CB2 4QD, UK.

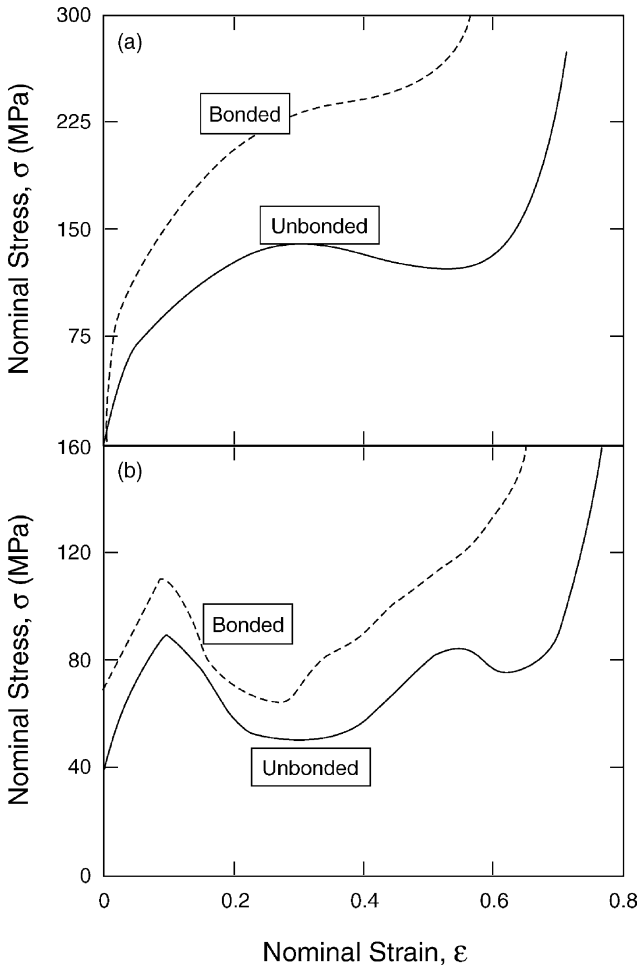

Fig. 6. Out-of-plane compressive stress vs. strain response of the $\bar{\rho} = 0.20$ square-honeycombs with cell aspect ratios (a) $H/L = 1$ and (b) $H/L = 5$. In each case, curves are shown for honeycombs that are bonded and not bonded to face-sheets.

for the unbonded stainless steel square-honeycomb at the same density with $H/L = 1$ (Fig. 10). The aluminum hexagonal-honeycombs have a lower peak stress and a more rapid softening beyond the peak. Each oscillation in the plateau region corresponds to the formation of a new fold in the cell walls. This difference in post-buckling response is attributed to the differing strain-hardening capacity of the cell wall material. That is, the high strain hardening of the stainless steel suppresses the formation of successive folds. The effect of relative density upon the peak strength of these Al alloy hexagonal-honeycombs is included in Fig. 7.

4. Buckling of honeycombs

4.1. Square-honeycombs

The buckling mode shown in Fig. 8 resembles torsional-axial buckling of a square tube with built-in top and bottom edges. Elastic buckling predominates at low relative densities [1], transitioning to plastic buckling at higher relative densities.

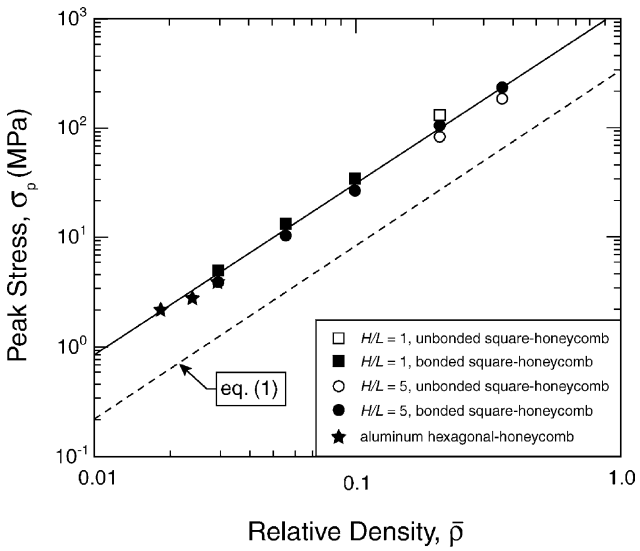

Fig. 7. The measured compressive peak stresses $\sigma_p = 5$ of the steel square and Al hexagonal-honeycomb specimens as a function of the relative density $\bar{\rho}$. The mean crushing strength prediction (1b) with $\sigma_y = 210$ MPa is also included.

4.1.1. Elastic buckling

The cells walls are treated as plates, height H, width L, and thickness t, simply supported along their vertical edges. The elastic buckling load P_c of such plates is [5]

$$P_c = \frac{k\pi^2}{6(1-\nu)} G \frac{t^3}{L}, \tag{4}$$

where G and ν are the elastic shear modulus and Poisson's ratio, respectively, of the plate material, and k a factor that depends upon the aspect ratio H/L as well as upon the boundary conditions at the top and bottom edges. For simply supported boundary conditions along the top and bottom edges, $k \approx 4.0$ provided that $H/L > 1$. Further k is insensitive to the boundary conditions along the top and bottom edges when $H/L \geq 3$. With the choice $k = 4.0$, the elastic bifurcation stress σ_c^e of the square-honeycombs becomes

$$\sigma_c^e = \frac{4\pi^2}{3(1-\nu)} G \left(\frac{t}{L}\right)^3 = \frac{\pi^2}{6(1-\nu)} G \bar{\rho}^3. \tag{5}$$

Note that Eq. (5) includes a dependence on ν, because the cell walls undergo longitudinal bending, in addition to twisting.

4.1.2. Plastic buckling

An extensive literature exists on the sensitivity of the plastic bifurcation load to the constitutive model (see, for example, the review of Hutchinson [6]). Flow theories with a smooth yield surface overestimate the bifurcation load. Deformation theories give closer agreement in the plastic range because they provide a more accurate representation

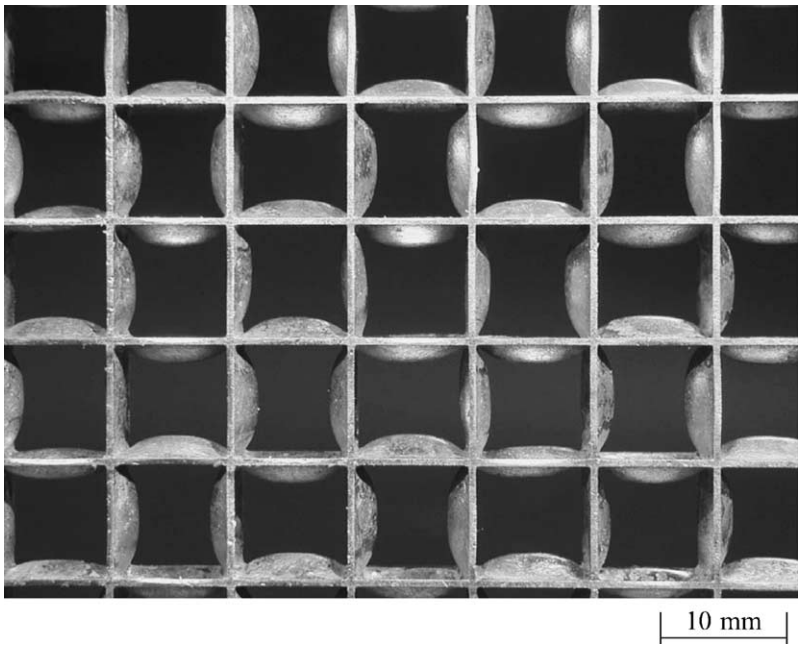

Fig. 8. A top view photograph of the unbonded $\bar{\rho} = 0.10$, 12×12 cells specimen ($H/L = 5$), compressed to a strain $\varepsilon \approx 0.1$. The photograph clearly shows an axial torsional buckling mode.

of the tangent moduli for mildly non-proportional loading. This finding has been rationalized in terms of crystal theories of plasticity. These theories suggest that a vertex develops at the loading point, with fixed tangent modulus for loading increments within a forward cone of the so-called "total loading" [7] or "fully active loading" [8], identical to that given by deformation theories. Flow theories give an excessively stiff response for non-proportional loading, such that large imperfections are needed to give buckling loads in agreement with experiment.

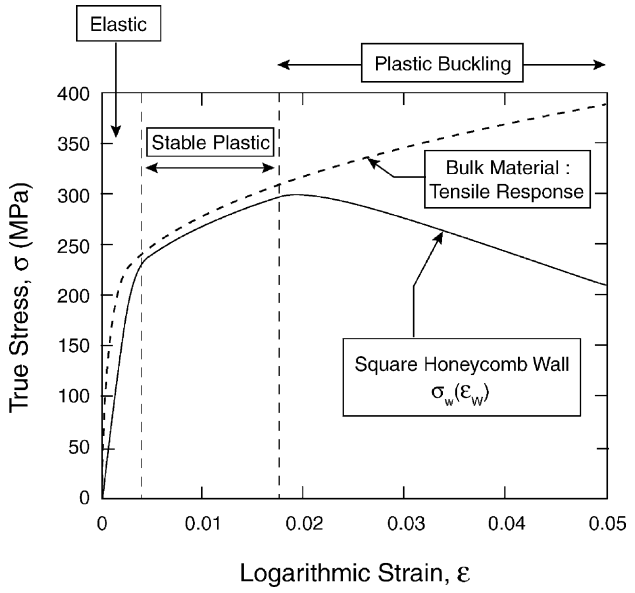

Fig. 9. A comparison between the tensile stress vs. strain response of the bulk 304 stainless steel and the inferred compressive stress vs. strain response of a cell wall of the square-honeycomb. The cell wall response is shown for the $\bar{\rho} = 0.10$, 12×12 cell square-honeycomb ($H/L = 5$) that has not been bonded to face-sheets.

The plastic bifurcation strength can be calculated from the elastic formula Eq. (5), which provided that the elastic shear modulus G and Poisson's ratio ν are each replaced by their incremental plastic values G_t and ν_t. In J2 deformation theory [9], the tangential shear modulus G_t degrades with uniaxial compressive stress σ_w in a cell wall element according to [6]

$$G_t = \frac{G}{1 + 3G(1/E_s - 1/E)}, \tag{6}$$

where E is the Young's modulus of the material and $E_s \equiv \sigma/\varepsilon$ is the secant modulus at the current value of σ_w. The tangent modulus E_t is likewise a function of σ_w and may be used to define ν_t:

$$\nu_t \equiv \frac{E_t - 2G_t}{2G_t}. \tag{7}$$

For simplicity, we assume that $\nu_t = 0.5$ is consistent with buckling deep in the plastic range. Then, the axial bifurcation stress σ_c^p is given via Eq. (5) as

$$\sigma_c^p = \frac{8\pi^2}{3} G_t \left(\frac{t}{L}\right)^3 = \frac{\pi^2}{3} G_t \bar{\rho}^3. \tag{8}$$

It is emphasized that G_t is evaluated from Eq. (6) by calculating E_s from the uniaxial true stress versus strain curve of the parent material at the uniaxial stress, $\sigma_c^p/\bar{\rho}$.

An analytical expression for σ_c^p may be obtained when the parent material has a linear hardening plastic response.

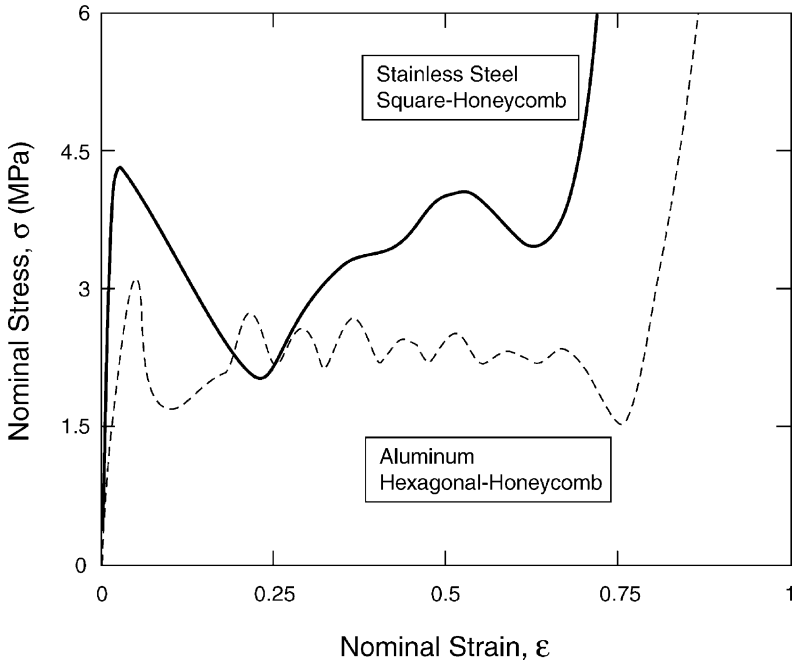

Fig. 10. A comparison between the unbonded compressive stress vs. strain response of typical stainless steel square-honeycomb and Al HexWeb hexagonal-honeycomb specimens. Both curves are shown for $\bar{\rho} = 0.03$ honeycombs with cell aspect ratio $H/L = 1$.

Then, the secant modulus E_s at bifurcation is given by

$$E_s = \frac{\sigma_c^p}{\bar{\rho}[\varepsilon_y + (\sigma_c^p/\bar{\rho} - \sigma_y)/E_t]}, \tag{9}$$

where ε_y is the yield strain of the parent material. Combining Eqs. (6), (8), and (9) gives the plastic bifurcation stress as,

$$\frac{\sigma_c^p}{\sigma_y} = \frac{\bar{E}[(\pi^2\bar{\rho}^3/3) - 3\bar{\rho}\varepsilon_y] + 3\bar{\rho}}{3 + \bar{E}\varepsilon_y(2\nu - 1)}, \tag{10}$$

where $\bar{E} \equiv E_t/\sigma_y$.

4.2. Hexagonal-honeycombs

The elastic buckling stress of the hexagonal-honeycombs with two cells walls per cell having double thickness is given by [1]

$$\sigma_c^e = \frac{12.1}{1-\nu} G\,\bar{\rho}^3. \tag{11}$$

Following an analysis similar to that detailed above, the plastic bifurcation stress σ_c^p of commercial hexagonal-honeycombs is

$$\sigma_c^p = 24.2 G_t \bar{\rho}^3, \tag{12}$$

and for honeycombs made from a parent material with a linear hardening modulus

$$\frac{\sigma_c^p}{\sigma_y} = \frac{\bar{E}[24.2\bar{\rho}^3 - 3\bar{\rho}\varepsilon_y] + 3\bar{\rho}}{3 + \bar{E}\varepsilon_y(2\nu - 1)}. \tag{13}$$

4.3. Comparison with measurements

A comparison between the buckling predictions and peak stress measurements (unbonded, $H/L = 5$) is shown in Fig. 11 by plotting the non-dimensional peak stress $\Sigma \equiv \sigma_p/(\sigma_y\bar{\rho})$ against relative density $\bar{\rho}$ with the elastic Poisson's ratio ν taken to be 0.3. The plastic bifurcation stresses are shown for three choices of the linear hardening modulus E_t, ranging from an ideally plastic solid ($\bar{E} = 0$) to a solid with a high hardening rate ($\bar{E} = 100$), as well as for the measured stress versus strain response (Fig. 3). The latter gives excellent agreement in the plastic range, when $\bar{\rho} \geq 0.05$. The linear hardening approximation also indicates reasonable agreement when $\bar{E} = 10$. The models predict the transition from elastic to plastic buckling at $\bar{\rho} \approx 0.035$.

The configuration with $\bar{\rho} = 0.03$, which is at the transition between elastic and plastic buckling, has peak stress about 30% below the predictions. This reduced strength is probably due to the presence of geometric imperfections: recall that the knock-down in bifurcation stress due to imperfections is greatest at the transition from the elastic to plastic buckling.

The prediction, Eq. (1b), is included in Fig. 11. A comparison with the ideally-plastic peak stress prediction ($\bar{E} = 0$) reveals that the ratio of peak to mean strength increases sharply with decreasing relative density; varying from ≈2 at $\bar{\rho} = 0.20$ to ≈6.4 at $\bar{\rho} = 0.10$. Recall that the mean stress prediction, Eq. (1b), refers to progressive folding, which was observed for the aluminum honeycomb (low strain-hardening capacity) but not for the stainless steel honeycomb (large strain-hardening capacity).

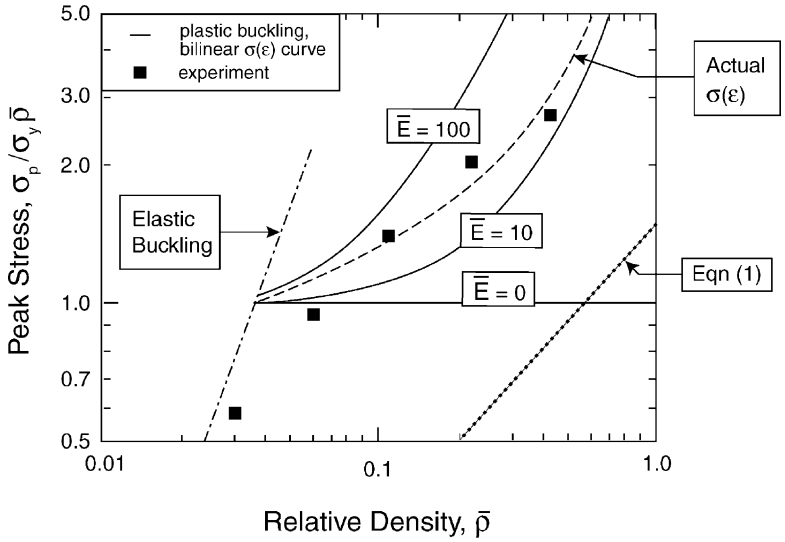

Fig. 11. A comparison between the measured and predicted values of the non-dimensional peak compressive strengths $\Sigma \equiv \sigma_p/(\sigma_y\bar{\rho})$ of the stainless steel square-honeycombs as a function of the relative density $\bar{\rho}$. The measured values are plotted for the $H/L = 5$ unbonded specimens.

Peak stress predictions for the hexagonal-honeycomb are plotted in Fig. 12 using $E = 70\,\text{GPa}$, $\nu = 0.3$, and $\sigma_y = 210\,\text{MPa}$, with no strain hardening as material properties of the 3003 grade aluminum from which the HexWeb honeycomb is manufactured. The predictions exceed the experimental measurements by a factor of up to two. We attribute this discrepancy to imperfections in HexWeb: the cell wall waviness was much less for the steel square-honeycomb, manufactured by the slotting method, than for the aluminum hexagonal-honeycomb, manufactured by the expansion method.

Finally, and surprisingly, a fit of the form

$$\Sigma \equiv \frac{\sigma_p}{\sigma_y\bar{\rho}} = 9.9\bar{\rho}^{0.75}, \tag{14}$$

characterizes the peak strengths of both the aluminum hexagonal and stainless steel square-honeycombs over a wide range of relative densities (Fig. 12). While no straightforward physical justification can be offered, it provides a useful rule for design purposes.

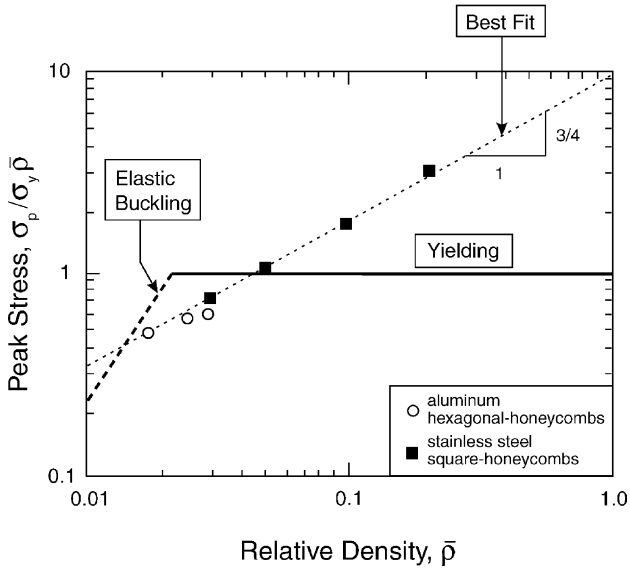

Fig. 12. A comparison between the measured non-dimensional peak compressive strengths $\Sigma \equiv \sigma_p/(\sigma_y\bar{\rho})$ of unbonded stainless steel square-honeycombs ($H/L = 1$) and the unbonded Al hexagonal-honeycombs as a function of the relative density $\bar{\rho}$. The elastic and ideally-plastic buckling predictions for the hexagonal-honeycombs have been included.

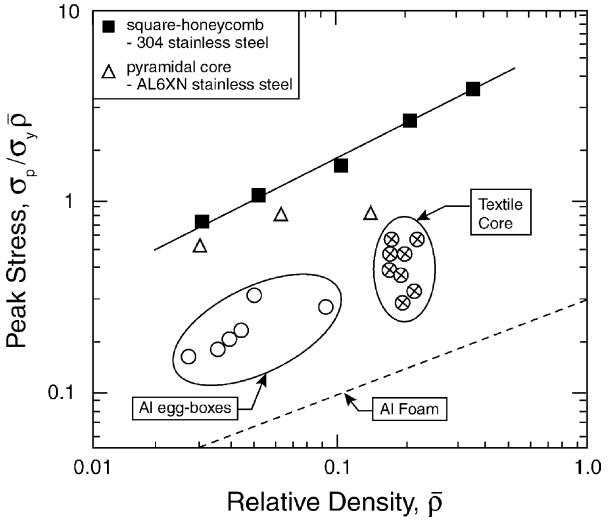

Fig. 13. A comparison between the measured non-dimensional peak compressive strengths $\Sigma \equiv \sigma_p/(\sigma_y\bar{\rho})$ of competing sandwich cores as a function of the relative density $\bar{\rho}$. The stainless steel square-honeycomb data shown are for the bonded $H/L = 5$ specimens tested in this study while the data for the other cores are taken from the literature.

5. Comparison with competing core designs

The performance of stainless steel square-honeycombs is compared with that for alternative cores in Fig. 13, which includes data for AL6XN stainless steel pyramidal cores [10], 316 stainless steel woven cores [11], aluminum egg-boxes [12], and aluminum alloy metal foams [13]. It is clear that the stainless steel square-honeycomb outperforms the other cores. The rationale is that the square-honeycomb is aligned with the loading axis, has few imperfections, and undergoes plastic buckling in an axial-torsional mode. The other topologies are misaligned with the loading direction and possess softer plastic buckling modes.

6. Concluding remarks

Square-honeycombs were manufactured by slotting together sheets of 304 stainless steel and then brazing the assembly. Five relative densities were tested in out-of-plane compression. The peak stress σ_p was found to be relatively insensitive to the ratio of the height of the honeycomb to cell size H/L, and unaffected by bonding to face-sheets, at least for relative densities of greatest practical relevance, $\bar{\rho} < 0.2$. An analytical model for buckling is shown to be in good agreement with the measured peak stress over the entire range of relative densities tested, $0.03 \leq \bar{\rho} \leq 0.36$.

Experimental measurements and predictions of buckling for aluminum hexagonal-honeycombs manufactured by the expansion process are reported. The measured strengths are below the analytical predictions due to imperfections introduced during manufacturing.

The square-honeycomb design exploits strain hardening extremely efficiently with the measured non-dimensional peak strength ratio Σ exceeding unity for $\bar{\rho} > 0.05$. In contrast, all other core topologies (pyramidal, woven, egg-box and metal foam) have $\Sigma < 1$ for all practical $\bar{\rho}$.

Acknowledgements

The authors are grateful to ONR for their financial support through US-ONR IFO grant number N00014-03-1-0283 on The Science and Design of Blast Resistant Sandwich Structures. FC acknowledges support from the Cambridge Commonwealth Trust and the Fonds québécois de la recherche sur la nature et les technologies.

References

[1] L.J. Gibson, M.F. Ashby, Cellular Solids, Structure and properties, 2nd ed., Cambridge University Press, Cambridge, 1997.
[2] T. Wierzbicki, W. Abramowicz, J. Appl. Mech. 50 (1983) 727–734.
[3] Z. Xue, J.W. Hutchinson, Int. J. Impact Eng. in press.
[4] N.A. Fleck, V.S. Deshpande, J. App. Mech. in press.
[5] S.P. Timoshenko, J.M. Gere, Theory of elastic stability, 2nd ed., McGraw Hill, New York, 1963.
[6] J.W. Hutchinson, in: C.-S. Yih (Ed.), Advances in applied Mechanics, vol 14, Academic Press, New York, 1974. pp. 67–144.
[7] B. Budiansky, J. Appl. Mech. 50 (1959) 259–264.
[8] R. Hill, J. Mech. Phys. Solids 15 (1967) 79–95.
[9] J. Lubliner, Plasticity theory, Macmillan, New York, 1990.
[10] M. Zupan, N.A. Fleck, 2004, in preparation.
[11] M. Zupan, V.S. Deshpande, N.A. Fleck, Eur. J. Mech. A: Solid, in press.
[12] M. Zupan, C. Chen, N.A. Fleck, Int. J. Mech. Sci. 45 (2003) 851–871.
[13] M.F. Ashby, A.G. Evans, N.A. Fleck, L.J. Gibson, J. W. Hutchinson, H.N.G. Wadley, Metal Foams: A Design Guide, Butterworth Heinemann, 2000.